



# Numerical Hydromagnetic Thermal Mechanism in Chemically Reacting Fluid Over a Radiative Melting UPHSR With Resistive Heating

Khalid Abdulkhaliq M. Alharbi<sup>1†</sup>, Adnan<sup>2\*†</sup>, Elsayed Tag-Eldin<sup>3</sup>, Mansour F. Yassen<sup>4,5</sup>, Naveed Ahmed<sup>6</sup> and Umar Khan<sup>7</sup>

<sup>1</sup>Mechanical Engineering Department, College of Engineering, Umm Al-Qura University, Makkah, Saudi Arabia, <sup>2</sup>Department of Mathematics, Mohi-ud-Din Islamic University, Nerian Sharif, Islamabad, Pakistan, <sup>3</sup>Faculty of Engineering and Technology, Future University in Egypt, New Cairo, Egypt, <sup>4</sup>Department of Mathematics, College of Science and Humanities in Al-Aflaj, Prince Sattam Bin Abdulaziz University, Al-Aflaj, Saudi Arabia, <sup>5</sup>Department of Mathematics, Faculty of Science, Damietta University, New Damietta, Egypt, <sup>6</sup>Department of Mathematics, Faculty of Sciences, HITEC University Taxila Cantt, Taxila, Pakistan, <sup>7</sup>Department of Mathematics and Statistics, Hazara University Mansehra, Mansehra, Pakistan

## OPEN ACCESS

### Edited by:

Muhammad Mubashir Bhatti,  
Shandong University of Science and  
Technology, China

### Reviewed by:

Muhammad Azam,  
Beijing Institute of Technology, China  
Mustafa Turkyilmazoglu,  
Hacettepe University, Turkey

### \*Correspondence:

Adnan  
adnan\_abbasi89@yahoo.com

### †ORCID:

Khalid Abdulkhaliq M. Alharbi  
<https://orcid.org/0000-0002-7290-8398>  
Adnan  
<https://orcid.org/0000-0003-0071-4743>

### Specialty section:

This article was submitted to  
Interdisciplinary Physics,  
a section of the journal  
Frontiers in Physics

Received: 05 June 2022

Accepted: 20 June 2022

Published: 29 August 2022

### Citation:

M. Alharbi KA, Adnan, Tag-Eldin E,  
F. Yassen M, Ahmed N and Khan U  
(2022) Numerical Hydromagnetic  
Thermal Mechanism in Chemically  
Reacting Fluid Over a Radiative Melting  
UPHSR With Resistive Heating.  
Front. Phys. 10:961671.  
doi: 10.3389/fphy.2022.961671

Heat transport over an upper paraboloid horizontal surface of revolution (UPHSR) has attracted much interest of the researchers and aero dynamists. The flow of fluid around the pointed surface of rocket, bullets, bonnet, and fighting aircrafts exhibits flows in which engineering parameters like shear stresses and Nusselt number significantly contributed. Therefore, the study of fluid comprising heat generation/absorption, Lorentz forces, and chemical reaction over a radiative UPHSR is conducted. The basic constitutive relations are transformed into dimensionless version via similarity variables and tackled numerically. The temperature  $\beta(\eta)$  extensively intensifies under stronger dissipation effects (Ec). Furthermore, Prandtl, Biot, and thermal radiations effects are observed to be of huge significance in the analysis of heat transfer. The concentration of the fluid decays for optimum Sc and  $\gamma$  over a UPHSR. The local rate of mass ( $-\phi'(0)$ ) and temperature ( $-\beta'(0)$ ) effectively increases for  $B_1$  and Sc, respectively.

**Keywords:** heat transfer, resistive heating, MHD, paraboloid of revolution, heat generation/absorption

## INTRODUCTION

The flow characteristics over an upper paraboloid horizontal surface of revolution (UPHSR) are significant and have attracted much interest from researchers and scientists. Flows of such a nature are seen across the tops of vehicles, the top face of bullets, and in aerodynamic phenomena. In this light, flow behavior over an UPHSR is a potential topic of interest in the field of fluid dynamics.

Keeping in mind the concept of the flow over an upper horizontal paraboloid surface of revolution, the researchers have focused on heat transport and fluid motion characteristics under various flow situations. Recently, Khan et al. [1] explored the behavior of Carreau liquid over a UPHSR. The model was introduced for bioconvection fluid by considering the influences of chemical reaction. The dimensionless comprising a new parametrization for Carreau fluid was treated by implementing Keller box techniques and decorated the results against the flow parameters. The reduction in the velocity of the bioconvection fluid against the stronger magnetic field was explored in the study. Moreover, they concluded that the stronger Prandtl effects reduced the fluid

temperature and thermophoresis, and Brownian effects led to an increment in the bioconvection fluid temperature.

In 2020, Santoshi et al. [2] presented the analysis of non-Newtonian fluid over a paraboloid of revolution. They adopted similarity transformations for the nondimensionalization of the model and then found impacts for various flow quantities, such as the Prandtl number, the Casson parameter, and the Weissenberg number for the flow properties. They indicated that the fluid motion drops by increasing the strength of the imposed magnetic field. Furthermore, augmentation to fluid temperature was reported against the Casson parameter. The influences of thermal radiations on the flow behavior are significant from an industrial and engineering point of view. In this regard, Makinde et al. [3] modeled a flow problem by comprising the thermal radiations effects in constitutive relations and attained a dimensionless version of the model via similarity transformation. They elaborated the results for the fluid temperature and motion and discussed them comprehensively.

In recent decades, researchers and scientists focused on exploring heat transport mechanisms in nanofluids [4]. Nanofluids are newly engineered colloidal suspensions of a host liquid and metallic nanomaterials. These have attracted attention among scientists and engineers due to their superior thermal performance compared to conventional liquids. The Lorentz forces significantly alters the characteristics of the nanofluids. Therefore, Animasaun et al. [5] conducted thermal transport in the nanofluids by considering the impacts of Lorentz forces [6] over an UPHSR. The colloidal mixture is made up of 29 nm CuO nanomaterials, and water was taken as the host liquid. It was assumed that the metallic nanoparticles were uniformly diluted in the host liquid. Significant alterations in the nanofluid velocity in the vicinity of UPHSR and augmentation in the thermal field were examined against a higher volumetric fraction.

Another significant analysis regarding the heat transport in the nanofluids over an UPHSR was conducted by Animasaun et al. [7] in 2019. They presented an analysis in the presence of Lorentz forces ([8]) and reported the fascinating flow behavior and thermal transport in the nanofluid against multiple flow quantities. The heat transfer and fluid motion for gyrotactic microorganisms in the presence of thermoelectric phenomena was reported in [9]. The authors examined the maximum fluid motion against Peclet and buoyancy parameters. To enhance the novelty of the study, they also incorporated the thermal radiation effects in the governing model and explored significant results for thermal performance in the flow of gyrotactic microorganisms.

The flow over a UPHSR exhibits a boundary layer flow and practiced in daily life and in engineering sides as well. The boundary layer is a thin layer of fluid in which the effects of viscosity are dominant. Such flows occur naturally around the wings of fish, flow of air around birds, and other occasions species. Therefore, the applications of such flows comprised in solar collectors, aeronautical engineering, and in aerodynamics. In 2017, Reddy et al. [10] introduced a computational model over an UPHSR by taking convective flow condition and Lorentz forces. To intensify the heat transport mechanism in the fluid, they used ferro magnetic nanomaterials and gained a colloidal

model. They examined a better heat transfer rate in ferrofluid in comparison with simple fluid. Moreover, the results for skin friction coefficient and the local thermal performance rate were elaborated in the form of numeric values.

The study of micropolar fluid over UPHSR in the presence of chemical reaction was carried out by Koriko and Animasaun [11] in 2017. They revealed that the temperature-dependent viscosity leads to an increment in the vertical fluid motion near the free stream, but the microrotation parameter declines near UPHSR. Furthermore, thermal radiation [12] had a significant influence on fluid thermal performance and walls shear stresses. The viscous dissipation effects greatly influence and alter the fluid characteristics over a finite or semi-infinite regions. In 2017, Ajayi et al. [13] detected the results for Casson dissipative fluid over a thermally radiative UPHSR. They reduced the constitutive relations for the momentum and energy into a dimensionless flow model, and then for mathematical analysis of the model, they utilized an RK scheme and portrayed the results in opposition to the flow parameters. They explored the significant effects of  $S_t$  on the wall shear stresses. Furthermore, significant investigation of the fluid characteristics over different geometries and flow conditions were reported in [14, 15] and in the literature cited therein.

The investigation of thermal performance in variety of nanofluids under bunch of physical conditions representing the fluid flow behavior at the boundaries with certain sources (magnetic field, thermal radiations [16], viscous dissipation, heat generation/absorption etc.) and activation energy is examined in [17–21]. The authors pointed that thermal radiations and activation energy are better sources to improve internal heat ability of the nanofluids particularly is Sutterby nanofluid. The exploration of fluid behavior in porous media is very significant and is of huge importance for underground reservoirs. In this context, a study is reported by Turkyilmazoglu [22] and engaged the study with novel aspects of solar heat, MHD, and internal thermal sources. The role of hybrid nanomaterials (Cu-Al<sub>2</sub>O<sub>3</sub>) for thermal enhancement in water under the impact of MHD, radiation source, and surface slip are discussed by Wahid et al. [23]. A recent analysis of heat transport was conducted by taking nonvariable magnetic field along a horizontal direction in [24].

## PROBLEM STATEMENT AND MATHEMATICAL MODELING

Consider two-dimensional, steady, and laminar flow of chemically reacting and electrically conducting Newtonian fluid past a thermally stratified upper horizontal surface of paraboloid of revolution place in Cartesian coordinate system. The coordinate axes are taken in such a way that  $x$  - axis is along the paraboloid surface and  $y$  - axis makes right angle with  $x$  - axis. Magnetic field  $\mathbf{B}$  is imposed perpendicularly to the UHSPR. It is considered that flow regimes are  $A(x+b)^{\frac{1-m}{2}} \leq y < \infty$ . Furthermore, fluid velocity at the paraboloid surface is of the form  $U_w = \frac{U_0}{(x+b)^m}$ . Here,  $b$  and  $m$  represent parameter related to stretchable sheet and velocity index parameter, respectively. The temperature of the fluid at

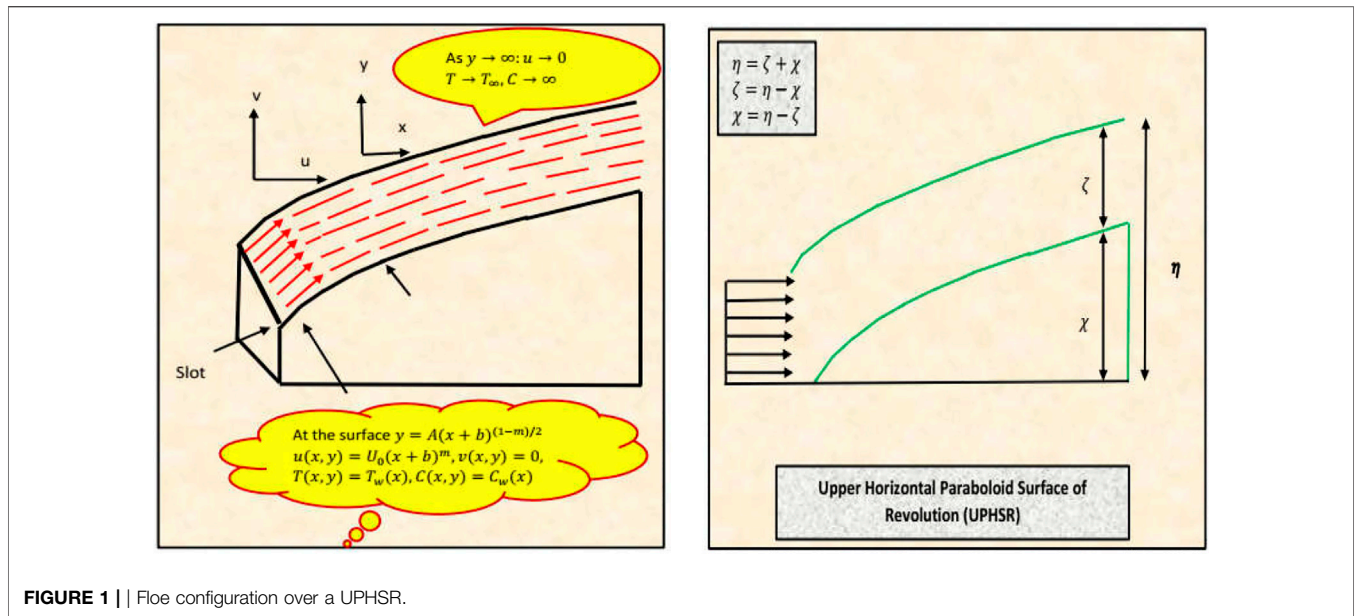


FIGURE 1 | Floe configuration over a UPHSR.

the surface is the function  $T_w(x) = A(x + b)^{\frac{m+1}{2}}$ . The physical model for the flow of chemically reacting fluid over a thermally stratified paraboloid surface of revolution is depicted in **Figure 1**.

The equations that govern the flow of chemically reacting and electrically conducting fluid over a paraboloid surface of revolution are the following [3, 13, 15]:

$$\frac{\partial u}{\partial x} + \frac{\partial v}{\partial y} = 0, \tag{1}$$

$$u \frac{\partial u}{\partial x} + v \frac{\partial u}{\partial y} = \frac{\mu}{\rho} \left( \frac{\partial^2 u}{\partial y^2} \right) - \frac{\sigma B^2}{\rho} u, \tag{2}$$

$$u \frac{\partial T}{\partial x} + v \frac{\partial T}{\partial y} = \frac{k}{\rho c_p} \left( \frac{\partial^2 T}{\partial y^2} \right) + \frac{Q_0(T_\infty - T_0)}{\rho c_p} (2.7128)^{-ny} \sqrt{\frac{m+1}{2}} \sqrt{\frac{U_0}{\nu}} (x+b)^{\frac{m-1}{2}} + \frac{\sigma B^2}{\rho c_p} (u^2) - \frac{16\sigma^* T_\infty^3}{3k^* \rho c_p} \left( \frac{\partial^2 T}{\partial y^2} \right), \tag{3}$$

$$u \frac{\partial C}{\partial x} + v \frac{\partial C}{\partial y} = D \left( \frac{\partial^2 C}{\partial y^2} \right) - k_1 (C - C_\infty). \tag{4}$$

The law of conservation of mass is given as in **Eq. 1**. The momentum and energy equations in the presence of magnetic field, internal heat source, and resistive heating are given in **Eqs 2, 3**, respectively. Furthermore, **Eq. 4** shows the mass transfer of the fluid. The dimensional physical quantities ingrained in **Eqs 1–4** are fluid density ( $\rho$ ), fluid dynamic viscosity ( $\mu$ ), imposed magnetic field ( $B$ ), specific heat capacity at constant pressure ( $c_p$ ), velocity stretching index ( $m$ ), Stefan Boltzmann constant ( $\sigma^*$ ), mean absorption coefficient ( $k^*$ ), ambient temperature  $T_\infty$ , mass diffusivity ( $D$ ), the rate of chemical reaction ( $k_1$ ),  $u$  is the velocity component along  $x$ -axis,  $v$  is the velocity of the fluid along  $y$ -axis,  $C$  is the fluid concentration, electrical conductivity ( $\sigma$ ), and thermal conductivity is  $k$ .

For our flow model, feasible set of boundary conditions for fluid motion, temperature, and concentration at the surface of paraboloid and away from the surface of paraboloid are listed in **Eqs 5, 6**. Physically, these conditions convey the message that velocity and concentration at  $y = 0$  is same as that of the surface. Furthermore, the UPHSR is subject to convective heat condition. As for as the fluid stream approaches to its final layer, the dynamics asymptotically decay.

At  $y = 0$ :

$$u(x, y) = U_w, v(x, y) = 0, -k \frac{\partial T}{\partial z} = h(T - T_w), C(x, y) = C_w(x), \tag{5}$$

At  $y \rightarrow \infty$ :

$$u(x, y) \rightarrow 0, T(x, y) \rightarrow T_\infty, C(x, y) \rightarrow C_\infty. \tag{6}$$

Furthermore, supporting self-similar variables are defined in the following way:

$$u = \frac{\partial \psi}{\partial y}, v = -\frac{\partial \psi}{\partial x}, \psi(x, y) = \sqrt{\frac{2\nu U_0}{m+1}} (x+b)^{\frac{m+1}{2}} f(\eta), \eta = \sqrt{\frac{(m+1)U_0}{2\nu}} (x+b)^{(m-1)/2} y, \beta^*(\eta) = \frac{T - T_\infty}{T_w - T_\infty}, \phi^*(\eta) = \frac{C - C_\infty}{C_w - C_\infty}. \tag{7}$$

In **Eq. 7**,  $\psi$  is the stream function and it gratifies the law of conservation of mass given in **Eq. 1**. After the differentiation of stream function w.r.t  $x$  and  $y$ , we arrive with the following  $u$  and  $v$  components of the velocity:

$$u = U_0(x + b)^m f'(\eta), \tag{8}$$

$$v = -\sqrt{\frac{2\gamma U_0}{(m+1)}} \frac{(m+1)}{2} (x+b)^{\frac{(m-1)}{2}} f(\eta). \tag{9}$$

The dimensional form of the flow model reduced into the following set of nonlinear differential equations by means of Eqs 7–9.

$$f''' - \left(\frac{2m}{m+1}\right) f'^2 + f f'' - M^2 f' = 0, \tag{10}$$

$$(1 + Rd)\beta^{*n} - \left(\frac{m-1}{m+1}\right) Pr \eta f' \beta^{*'} + Pr f \beta^{*'} + \frac{2Pr\gamma_1}{(m+1)} (2.7128)^{-m\eta} + \frac{2PrEcM^2}{(m+1)} f'^2 = 0, \tag{11}$$

$$\phi^{*n} - \left(\frac{m-1}{m+1}\right) Sc \eta f' \phi^{*'} + Sc f \phi^{*'} - \gamma Sc \phi = 0. \tag{12}$$

Here, it is important to mention that the lower value of  $\gamma$  is not at the infant point of the slot. In this condition, it is impossible to apply all the boundary conditions in Eq. 5 at  $y = 0$ . Applying  $A = (x + b)^{\frac{m+1}{2}}$  smaller value of  $\gamma$  is almost correspond to the smaller values of the dimensionless variable  $\eta$ . For this purpose, a suitable value for  $\eta$  is taken in the following way:

$$\eta = A \sqrt{\frac{(m+1)U_0}{2\gamma}} = \chi. \tag{13}$$

This implies that suitable auxiliary conditions obtain at the surface for feasible scale at  $\eta = \chi$ . Thus, boundary conditions are reduced into the following manner:

$$f'(\chi) = 1, f(\chi) = \chi \left[ \frac{1-m}{1+m} \right], \beta^{*'}(\chi) = B_i(\beta^*(\chi) - 1), \phi^*(\chi) = 1, \tag{14}$$

$$f'(\chi) \rightarrow 0, \beta^*(\chi) \rightarrow 0, \phi^*(\chi) \rightarrow 0. \tag{15}$$

Furthermore, to restrict the domain  $[\chi, \infty)$  to  $[0, \infty)$ , we use  $F(\zeta) = F(\eta - \chi) = f(\eta)$ ,  $\beta(\zeta) = \beta(\eta - \chi) = \beta^*(\eta)$ , and  $\phi(\zeta) = \phi(\eta - \chi) = \phi^*(\eta)$ . Thus, Eqs 10–12 reduce into the following set of nonlinear ordinary differential equations:

$$F''' - \left(\frac{2m}{m+1}\right) F'^2 + FF'' - M^2 F' = 0, \tag{16}$$

$$(1 + Rd)\beta'' - \left(\frac{m-1}{m+1}\right) Pr \eta F' \beta' + Pr F \beta' + \frac{2Pr\gamma_1}{(m+1)} (2.7128)^{-m\zeta} + \frac{2PrEcM^2}{(m+1)} F'^2 = 0, \tag{17}$$

$$\phi'' - \left(\frac{m-1}{m+1}\right) Sc \eta F' \phi' + Sc F \phi' - \gamma Sc \phi = 0. \tag{18}$$

For our flow problem, nondimensional boundary conditions are set in the following manner:

$$At \zeta = 0:$$

$$F'(\zeta) = 1, F(\zeta) = \chi \left[ \frac{1-m}{1+m} \right] \beta'(\zeta) = B_i(\beta(\zeta) - 1), \phi(\zeta) = 1. \tag{19}$$

$$At \zeta \rightarrow \infty:$$

$$F'(\zeta) \rightarrow 0, \beta(\zeta) \rightarrow 0, \phi(\zeta) \rightarrow 0. \tag{20}$$

The non-dimensional physical quantities appeared in Eqs 16–18 are as follows:

$$M^2 = \frac{\sigma B_0^2}{\rho}, Pr = \frac{\gamma C_p}{k}, Ec = \frac{U_0(x+b)^{m+1}}{c_p(T_w - T_\infty)} \text{ and } Sc = \frac{\nu}{D}$$

Quantities of physical and practical interest, such as skin friction coefficient, local heat transfer, and mass transfer gradients in nondimensional form, are as follows:

$$C_F \sqrt{Re_x} = F''(0), Nu(Re_x)^{-\frac{1}{2}} = -\beta'(0), Sh(Re_x)^{-\frac{1}{2}} = -\phi'(0). \tag{21}$$

Here,  $Re_x = \frac{U_\infty(x+b)}{\nu}$  and is known as the local Reynold number.

### MATHEMATICAL ANALYSIS

For our flow model, it is very difficult to perform analytical computations, or such solutions may not even exist. Thus, for the flow model, we adopted numerical technique called the Runge-Kutta scheme [25–27]. First, we transformed under consideration flow model in a system of first-order initial value problem, and then computations are carried out by means of Mathematica 10.0. To obtain the first-order initial value problem, we made the following substitutions:

$$y_1 = F, y_2 = F', y_3 = F'', y_4 = \beta, y_5 = \beta', y_6 = \phi, y_7 = \phi'. \tag{22}$$

The system given in Eqs 16–18 can be written in the following manner:

$$F''' = \left(\frac{2m}{m+1}\right) F'^2 - FF'' + M^2 F', \tag{23}$$

$$\beta'' = \left(\frac{1}{1 + Rd}\right) \left[ \left(\frac{m-1}{m+1}\right) Pr \eta F' \beta' - Pr F \beta' - \frac{2Pr\gamma_1}{(m+1)} (2.7128)^{-m\zeta} - \frac{2PrEcM^2}{(m+1)} F'^2 \right], \tag{24}$$

$$\phi'' = \left(\frac{m-1}{m+1}\right) Sc \eta F' \phi' - Sc F \phi' + \gamma Sc \phi. \tag{25}$$

With the help of the substitution given in Eq. 22, we arrive with the following system of first-order initial value problem:

**TABLE 1 |** Numerical solutions for the velocity, temperature, and concentration fields.

<b>M = 0.8, Ec = 0.5, Pr = 0.5, Rd = 0.5</b>			
$\eta$	$F'(\eta)$	$\beta(\eta)$	$\phi(\eta)$
0.0	1.0000000000	1.0000000000	0.4146310423
0.5	0.7662305531	0.9191915518	0.2819022951
1.0	0.5464022186	0.8030584935	0.1821525111
1.5	0.3661580056	0.6751297664	0.1141150633
2.0	0.2324718931	0.5494943249	0.0701936150
2.5	0.1402323502	0.4325166571	0.0425405624
3.0	0.0799362225	0.3261851156	0.0252387806
3.5	0.0422413076	0.2305211258	0.0143625937
4.0	0.0196724145	0.1448369037	0.0074459103
4.5	0.0068222641	0.0682750712	0.0029695571
5.0	$-2.24747564 \times 10^{-8}$	$-3.558369439 \times 10^{-8}$	$2.504364957 \times 10^{-8}$

$$\begin{bmatrix} y_1' \\ y_2' \\ y_3' \\ y_4' \\ y_5' \\ y_6' \\ y_7' \end{bmatrix} = \begin{bmatrix} y_2 \\ y_3 \\ \left(\frac{2m}{m+1}\right)y_2^2 - y_1y_3 + M^2y_2 \\ y_5 \\ \left(\frac{1}{1+Rd}\right)\left[\left(\frac{m-1}{m+1}\right)Pr \right. \\ \left. \left[\eta y_2y_5 - y_1y_5 - \frac{2y_1}{(m+1)}(2.7128)^{-\zeta n} - \frac{2EcM^2}{(m+1)}y_2^2\right] \right] \\ y_7 \\ \left(\frac{m-1}{m+1}\right)Sc\eta y_2y_7 - Scy_1y_7 + \gamma Scy_6 \end{bmatrix} \quad (26)$$

The set of initial conditions is as follows:

$$\begin{bmatrix} y_1 \\ y_2 \\ y_3 \\ y_4 \\ y_5 \\ y_6 \\ y_7 \end{bmatrix} = \begin{bmatrix} 1 \\ \chi \left[ \frac{1-m}{1+m} \right] \\ l_1 \\ B_i(l_2 - 1) \\ l_3 \\ 1 \\ l_4 \end{bmatrix} \quad (27)$$

Here,  $l_i$  (for  $i = 1, 2, 3, 4$ ) are unknown. Using Mathematica 10.0, we compute the tabulated results for the velocity, temperature, and concentration fields (**Table 1**):

## RESULTS AND DISCUSSION

This section explores the influence of various dimensionless physical quantities appearing in the flow in terms of the velocity, temperature, and concentration of the fluid. These quantities play significant role in the flow regimes. In this study, these parameters are magnetic number, Prandtl number, Eckert number, radiation parameter, chemical reaction parameter, Schmidt number, and Biot number. For this purpose, **Figures 2–8** are portrayed. Three-dimensional scenario of the flow regimes is also provided. Furthermore, in this section numerical computations for skin friction coefficient, local rate of heat, and mass transfer are carried out for varying physical quantities.

**Figures 2A,B** illustrate the impact of the velocity index parameter  $m$  and Lorentz force on the velocity field and the velocity gradient, respectively. The velocity index parameter shows the decline in the fluid velocity. The activity of the fluid decreases rapidly in the region  $0.1 \leq \zeta \leq 1.0$ . As we move beyond this region, velocity field of the fluid starts decreasing asymptotically. The variations in velocity gradient  $F'(\zeta)$  also decreases due to increasing the velocity index parameter  $m$ . In the vicinity of the paraboloid surface, the velocity gradient shows almost inconsequential variations. However, as we move away from the surface of paraboloid, the velocity gradient starts decreasing rapidly. Furthermore, three-dimensional view of the velocity field  $F(\zeta)$  and the velocity gradient  $F'(\zeta)$  is depicted in **Figures 3A,B**, respectively, due to varying velocity index parameter  $m$  and magnetic number  $M$ .

The effects of the Eckert number  $Ec$  and velocity index parameter  $m$  on the fluid temperature and temperature gradient are portrayed in **Figures 4A,B**, respectively. It is noted for increasing  $Ec$  fluid temperature increases rapidly in the vicinity of the paraboloid surface. Far away from the surface, the influence of the Eckert number on the fluid temperature is almost inconsequential, and temperature vanishes asymptotically. On the other hand, temperature gradient shows reverse behavior for increasing the Eckert number. In the region  $0.5 \leq \zeta \leq 2.0$ , temperature gradient  $\beta'(\zeta)$  decreases rapidly. The velocity index parameter  $m$  against the fluid temperature and temperature gradient, respectively. For the higher velocity index parameter  $m$  thermal field and thermal gradient field decreases rapidly. **Figures 5A,B** elucidates 3D view of the temperature field  $\beta(\zeta)$  and thermal gradient field  $\beta'(\zeta)$ , respectively.

The next set of figures highlight the variations in fluid temperature  $\beta(\zeta)$  and temperature gradient field  $\beta'(\zeta)$  for arising Prandtl and Biot numbers, respectively. From **Figure 6A**, it can be seen that for higher Prandtl value, thermal field  $\beta(\zeta)$  increases rapidly near the paraboloid surface. However, after  $\zeta > 2$ , the fluid temperature begins to decrease and vanishes asymptotically beyond  $\zeta > 12$ . Similarly, a rapidly falling temperature gradient  $\beta'(\zeta)$  is noted near the surface. The Biot number  $B_i$  opposes the fluid temperature. This behavior of the fluid can be seen

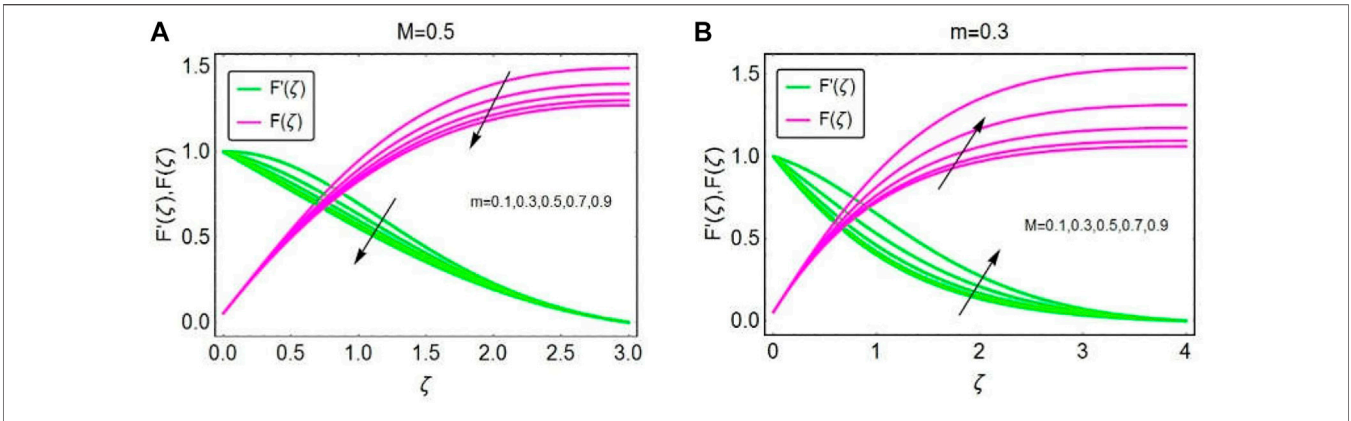


FIGURE 2 | Influence of (A)  $m$  and (B)  $M$  on the velocity field.

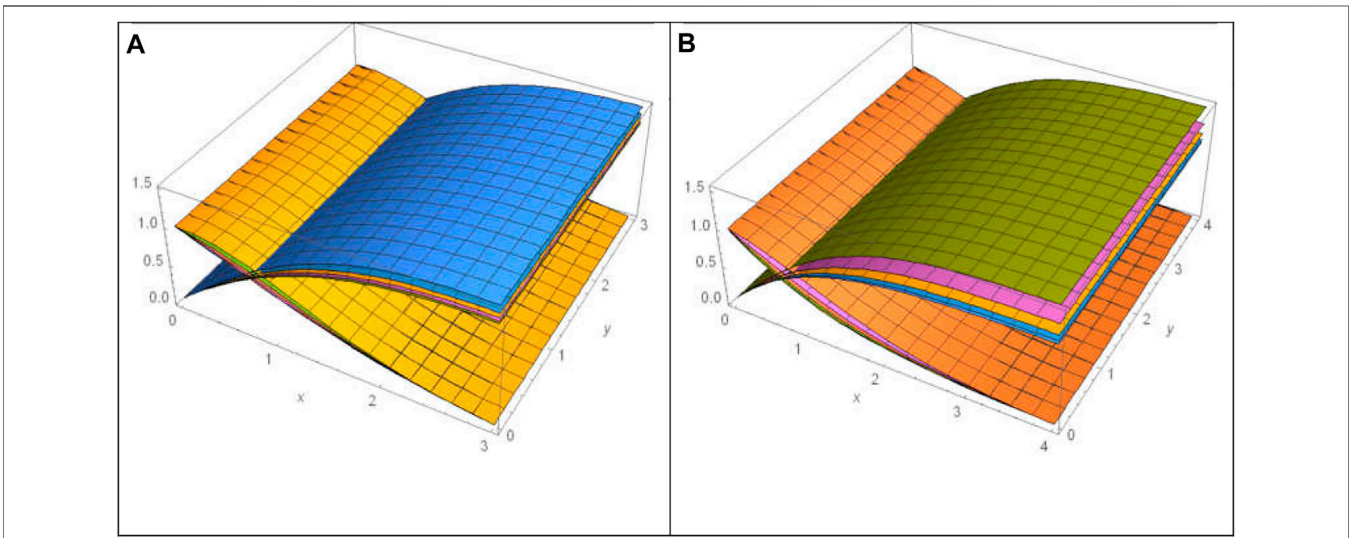


FIGURE 3 | 3D view for (A)  $m$  and (B)  $M$  on the velocity field.

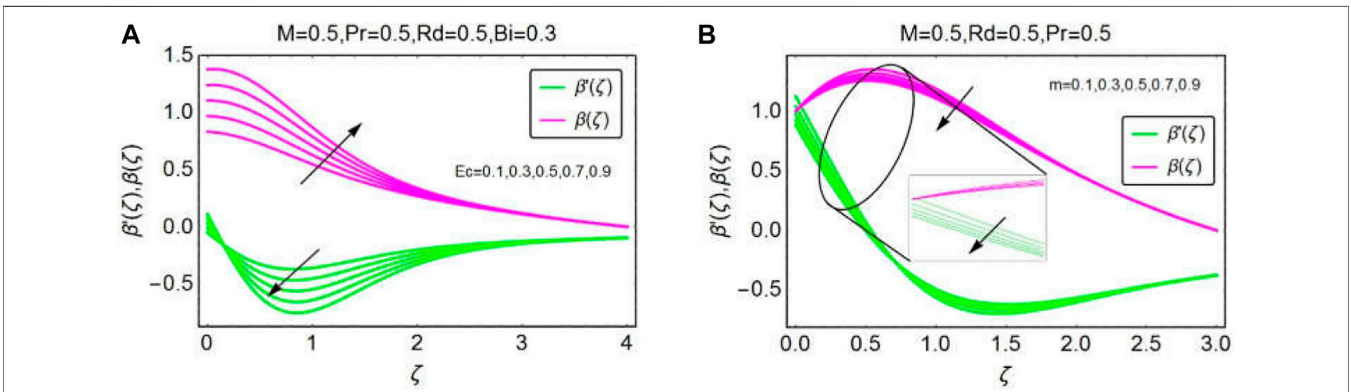


FIGURE 4 | Influence of (A)  $Ec$  and (B)  $m$  on  $\beta(\zeta)$  and  $\beta'(\zeta)$ .

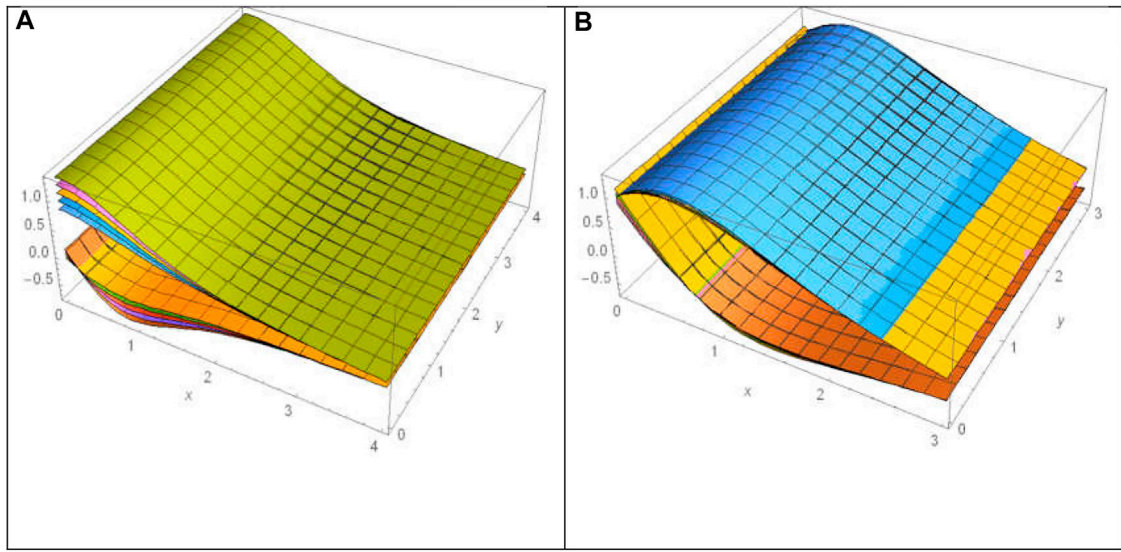


FIGURE 5 | 3D view of  $\beta(\zeta)$  and  $\beta'(\zeta)$  for (A)  $Ec$  and (B)  $m$ .

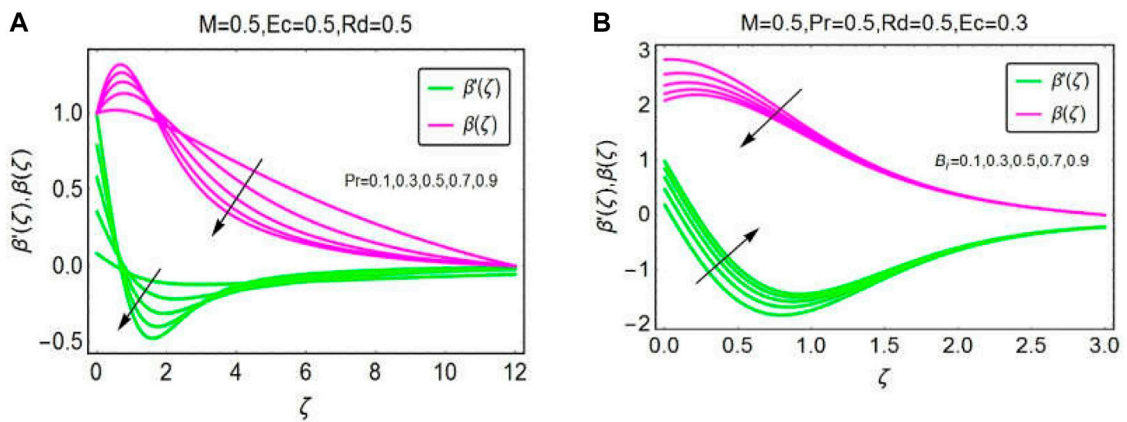


FIGURE 6 | Influence of (A)  $Pr$  and (B)  $B_1$  on  $\beta(\zeta)$  and  $\beta'(\zeta)$ .

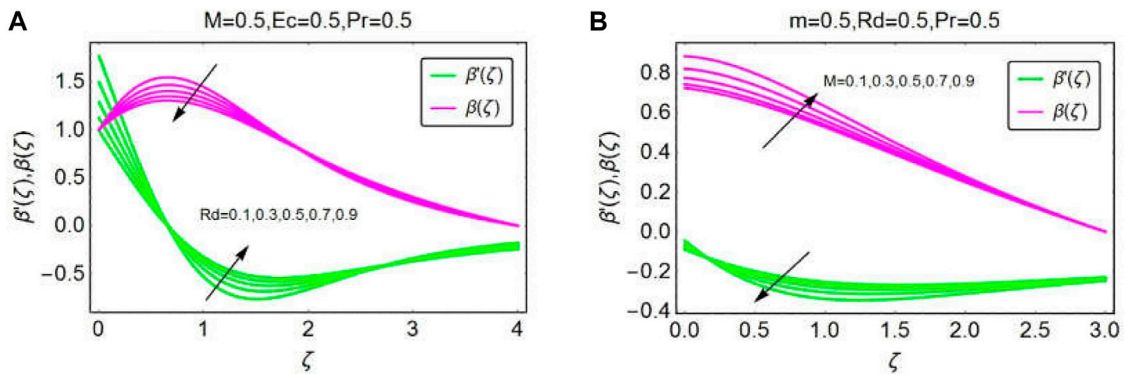


FIGURE 7 | Influence of (A)  $Rd$  and (B)  $M$  on  $\beta(\zeta)$  and  $\beta'(\zeta)$ .

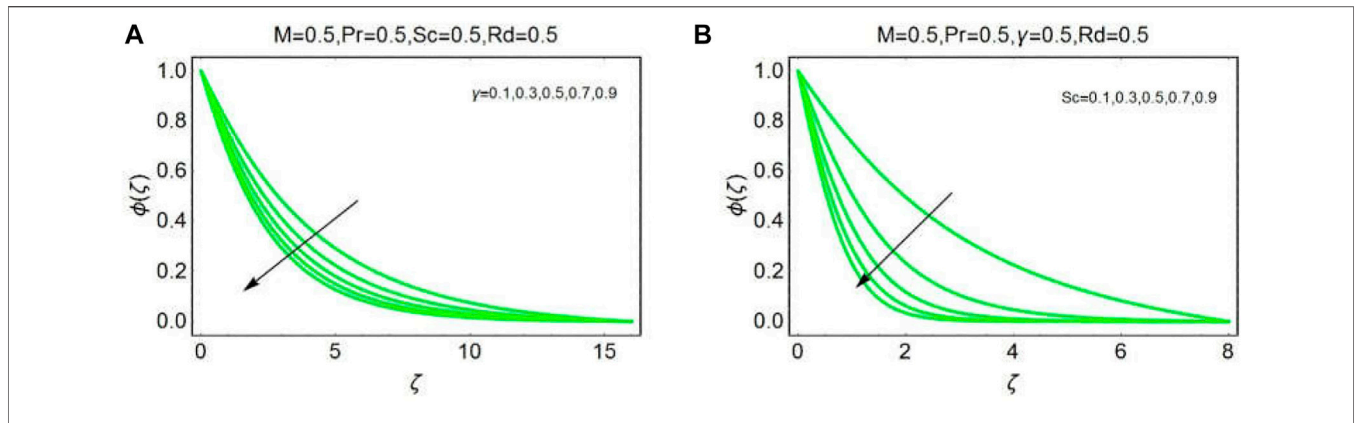


FIGURE 8 | Influence of (A)  $\gamma$  and (B)  $Sc$  on  $\phi(\zeta)$ .

TABLE 2 | Numerical values for skin friction coefficient and local Nusselt and Sherwood numbers.

$m$	$M$	$Pr$	$Ec$	$B_i$	$Sc$	$\gamma$	$F''(0)$	$-\beta'(0)$	$-\phi'(0)$
0.1	0.3	0.3	0.3	0.3	0.3	0.3	-0.744088	0.057493	0.50555
0.2							-0.805269	0.063379	0.49437
0.3							-0.854406	0.068558	0.48551
0.1	0.5						-0.63036	0.058409	0.51649
	0.7						-0.433181	0.059690	0.53641
	0.9						-0.111974	0.059664	0.56915
	0.3	0.5						0.030813	
		0.7						0.012479	
		0.9						0.000392	
		0.3	0.5					0.056514	
			0.7					0.055534	
			0.9					0.054555	
			0.3	0.5				0.073178	
				0.7				0.082867	
				0.9				0.089446	
				0.3	0.5				0.689998
					0.7				0.857216
					0.9				1.009620
					0.3	0.5			0.567593
						0.7			0.623424
						0.9			0.674436

from Figure 6B. Over a more convectively heated surface, the fluid temperature decreases rapidly. This decreasing behavior of the fluid is very clear in the vicinity of the paraboloid surface. Furthermore, the Biot number favors the thermal gradient profile near the surface, and the asymptotic behavior is investigated away from the surface for both fluid temperature and its gradient.

The influence of thermal radiation and the magnetic parameter  $M$  on fluid temperature and its gradient  $\beta'(\zeta)$  are illustrated in Figures 7A,B. The radiation parameter shows fascinating behavior in the fluid temperature  $\beta(\zeta)$  and temperature gradient  $\beta'(\zeta)$ . It is noted that fluid temperature decreases for stronger radiation parameter. These effects can be seen in the region  $\zeta = 1$ . On the surface of the paraboloid of revolution, the influence of  $Rd$  on  $\beta(\zeta)$  is noted almost

inconsequential. Away from the surface, decrement in the fluid temperature become slow. The radiation parameter favors the temperature gradient profile  $\beta'(\zeta)$ . These effects are very clear in the portion  $1.0 \leq \zeta \leq 2.0$ . Beyond this region, the temperature gradient profile shows almost negligible behavior for imposed thermal radiation. The influence of Lorentz forces on fluid temperature depicted in Figure 8B. It is observed that imposed magnetic field favors the fluid temperature on the surface of paraboloid. Away from the surface, the increasing activity of the temperature profile becomes almost inconsequential. On the other hand, temperature gradient field  $\beta'(\zeta)$  decreases for stronger magnetic fields.

The influence of chemical reaction parameter  $\gamma$  and Schmidt number  $Sc$  on mass transfer profile illustrated in Figures 8A,B, respectively. To increase  $\gamma$  and  $Sc$ , the mass transfer decreases and

**TABLE 3** | Comparison for  $F''(\eta_{=0})$  with existing data.

$m$	Current Computation	[28]	[29]
0.1	-0.8681133	-0.8671009	-0.8681133
0.2	-0.859491	-0.8654053	-0.859491
0.3	-0.852225	-0.8584863	-0.852225

rapid decrement is investigated. In the case of Schmidt number, these variations are much more rapid than those of the chemical reaction parameter.

The variations in skin friction coefficient, local rate of heat transfer (local Nusselt number), and local rate of mass transfer (Sherwood number) are described in **Table 2** due to variations in pertinent flow parameters. It is noted that for increasing velocity index parameter  $m$  stronger magnetic parameter  $M$ , the skin friction coefficient increases absolutely. The Biot number enhanced the local rate of heat transfer and in more dissipative flow (increasing Eckert number), the local Nusselt number starts decreasing. Furthermore, the Schmidt number and chemical reaction parameter  $\gamma$  favor local mass transfer (Sherwood number).

## STUDY VALIDATION

The current investigation is validated through numerical comparison with previously described data in the literature. This was carried out using certain assumptions for the model, and a fine comparison between both the current and reported results for  $F''(0)$  was found. The computation is performed for  $m = 0.1, 0.2, 0.3$ . Furthermore, thermal radiations and chemical reaction effects were neglected in the comparison, and these results are listed in **Table 3**.

## REFERENCES

- Khan M, Hussain A, Malik MY, Salahuddin T. Biconvection Flow of Carreau Fluid over an Upper Paraboloid Surface: A Computational Study. *Results Phys* (2017) 7:4050–7. doi:10.1016/j.rinp.2017.10.023
- Santoshi PN, Reddy GVR, Padma P. Flow Features of Non-newtonian Fluid through a Paraboloid of Revolution. *Int J Appl Comput Math* (2020) 6. doi:10.1007/s40819-020-00828-z
- Makinde OD, Sandeep N, Ajayi TM, Animasaun IL. Numerical Exploration of Heat Transfer and Lorentz Force Effects on the Flow of MHD Casson Fluid over an Upper Horizontal Surface of a Thermally Stratified Melting Surface of a Paraboloid of Revolution. *Int J Nonlinear Sci Numer Simulation* (2018) 19: 93–106. doi:10.1515/ijnsns-2016-0087
- Adnan Ahmed N, Mohyud-Din ST, Hamadneh NN, Khan I, Andualet. The Dynamics of H<sub>2</sub>O Suspended by Multiple Shaped Cu Nanoadditives in Rotating System. *J Nanomater* (2021) 2021:1–11. doi:10.1155/2021/7299143
- Animasaun IL, Mahanthesh B, Jagun AO, Bankole TD, Sivaraj R, Shah NA, et al. Significance of Lorentz Force and Thermoelectric on the Flow of 29 Nm CuO-Water Nanofluid on an Upper Horizontal Surface of a Paraboloid of Revolution. *J Heat Transfer* (2019) 141(2). doi:10.1115/1.4041971
- Khan W, Khan U, Adnan Ullah B, Khan I, Alqahtani AM, et al. The Effects of Magneto-Radiative Parameters on the Heat Transfer Mechanism in H<sub>2</sub>O

## CONCLUSION

A novel study regarding the heat and mass transfer over an UPHSR subject to magnetic field, radiation effects, chemical reaction, and internal heat source is reported. The results for the flow field demonstrated and indicated that:

- The velocity index parameter opposes the fluid motion inside the flow field.
- Thermal field  $\beta(\eta)$  increases prominently in the locality of the surface under high dissipation effects.
- The more chemically reacting fluid and increasing Schmidt number,  $\phi(\zeta)$  decreases.
- The skin friction coefficient shows absolutely increasing behavior for  $m$  and  $M$ , respectively.
- The local heat and mass transfer rate intensify by enhancing convection from the surface and Schmidt effects.

## DATA AVAILABILITY STATEMENT

The raw data supporting the conclusion of this article will be made available by the authors, without undue reservation.

## AUTHOR CONTRIBUTIONS

All authors listed have made a substantial, direct, and intellectual contribution to the work and approved it for publication.

## ACKNOWLEDGMENTS

The authors would like to thank the Deanship of Scientific Research at Umm Al-Qura University for supporting this work by Grant Code: (22UQU4310392DSR18).

Composed by Cu-Al<sub>2</sub>O<sub>3</sub> Hybrid Nanomaterial: Numerical Investigation. *Math Probl Eng* (2022) 2022:1–10. doi:10.1155/2022/3098781

- Animasaun IL, Mahanthesh B, Jagun AO, Bankole TD, Sivaraj R, Shah NA, et al. Significance of Lorentz Force and Thermoelectric on the Flow of 29 Nm CuO-Water Nanofluid on an Upper Horizontal Surface of a Paraboloid of Revolution. *J Heat Transfer-transactions Asme* (2019) 141. doi:10.1115/1.4041971
- Abbasi A, Ahmed N, Mohyud-Din ST. Flow of Magneto-Nanofluid over a Thermally Stratified Bi-directional Stretching Sheet in the Presence of Ohmic Heating: A Numerical Study of Particle Shapes. *Eng Computations* (2017) 34(8):499–2513.
- Sivaraj R, Animasaun IL, Olabiyi AS, Saleem S, Sandeep N. Gyrotactic Microorganisms and Thermoelectric Effects on the Dynamics of 29 Nm CuO-Water Nanofluid over an Upper Horizontal Surface of Paraboloid of Revolution. *Mmms* (2018) 14:695–721. doi:10.1108/MMMS-10-2017-0116
- Ramana Reddy JV, Sugunamma V, Sandeep N. Enhanced Heat Transfer in the Flow of Dissipative Non-newtonian Casson Fluid Flow over a Convectively Heated Upper Surface of a Paraboloid of Revolution. *J Mol Liquids* (2017) 229: 380–8. doi:10.1016/j.molliq.2016.12.100
- Koriko LIOK, Animasaun IL. New Similarity Solution of Micropolar Fluid Flow Problem over an UHSPR in the Presence of Quartic Kind of Autocatalytic Chemical Reaction. *Front Heat Mass Transfer* (2017) 8(26). doi:10.5098/hmt.8.26

12. Ahmed N, Adnan Khan U, Khan I, Murtaza R, Hussain I, et al. A Novel Investigation and Hidden Effects of MHD and Thermal Radiations in Viscous Dissipative Nanofluid Flow Models. *Front Phys* (2020) 8. doi:10.3389/fphy.2020.00075
13. Ajayi TM, Omowaye AJ, Animasaun IL. Viscous Dissipation Effects on the Motion of Casson Fluid over an Upper Horizontal Thermally Stratified Melting Surface of a Paraboloid of Revolution: Boundary Layer Analysis. *J Appl Maths* (2017) 2017:1–13. doi:10.1155/2017/1697135
14. Kumaran G, Sandeep N, Animasaun IL. Computational Modeling of Magnetohydrodynamic Non-newtonian Fluid Flow Past a Paraboloid of Revolution. *Alexandria Eng J* (2018) 57:1859–65. doi:10.1016/j.aej.2017.03.019
15. Abegunrin OA, Animasaun IL, Sandeep N. Insight into the Boundary Layer Flow of Non-newtonian Eyring-Powell Fluid Due to Catalytic Surface Reaction on an Upper Horizontal Surface of a Paraboloid of Revolution. *Alexandria Eng J* (2018) 57:2051–60. doi:10.1016/j.aej.2017.05.018
16. Adnan Ashraf W, Junaid Anjum H, Mousa IM, Mehrez S. Energy Transformation and Entropy Investigation in the Nanofluid Composed by  $\gamma$ -Nanomaterial over a Permeable Convective Surface with Solar Thermal Radiation: A Numerical Analysis. *Front Energ Res.* (2022) 10. doi:10.3389/fenrg.2022.888389
17. Azam M. Effects of Cattaneo-Christov Heat Flux and Nonlinear thermal Radiation on MHD Maxwell Nanofluid with Arrhenius Activation Energy. *Case Stud Therm Eng* (2022) 34:102048. doi:10.1016/j.csite.2022.102048
18. Azam M, Abbas Z. Recent Progress in Arrhenius Activation Energy for Radiative Heat Transport of Cross Nanofluid over a Melting Wedge. *Propulsion Power Res* (2021) 10(4):383–95. doi:10.1016/j.jppr.2021.11.004
19. Azam M, Mabood F, Khan M. Bioconvection and Activation Energy Dynamisms on Radiative Sutterby Melting Nanomaterial with Gyrotactic Microorganism. *Case Stud Therm Eng* (2022) 30:101749. doi:10.1016/j.csite.2021.101749
20. Azam M. Bioconvection and Nonlinear thermal Extrusion in Development Ofchemically Reactive Sutterby Nano-Material Due to Gyrotactic Microorganisms. *Int Commun Heat Mass Transfer* (2022) 130:105820. doi:10.1016/j.icheatmasstransfer.2021.105820
21. Azam M, Xu T, Mabood F, Khan M. Non-linear Radiative Bioconvection Flow of Cross Nano-Material with Gyrotactic Microorganisms and Activation Energy. *Int Commun Heat Mass Transfer* (2021) 127:105530. doi:10.1016/j.icheatmasstransfer.2021.105530
22. Turkyilmazoglu M. MHD Natural Convection in Saturated Porous media with Heat Generation/absorption and thermal Radiation: Closed-form Solutions. *Arch Mech* (2019) 71(1):49–64.
23. Wahid NS, Md Arifin N, Turkyilmazoglu M, Hafidzuddin MEH, Abd Rahmin NA. MHD Hybrid Cu-Al<sub>2</sub>O<sub>3</sub>/Water Nanofluid Flow with Thermal Radiation and Partial Slip Past a Permeable Stretching Surface: Analytical Solution. *JNanoR* (2020) 64:75–91. doi:10.4028/www.scientific.net/JNanoR.64.75
24. Turkyilmazoglu M. Flow and Heat over a Rotating Disk Subject to a Uniform Horizontal Magnetic Field. *Z für Naturforschung A* (2022). doi:10.1515/zna-2021-0350
25. Adnan Ashraf W, Khan I, Anduaem M. Thermal Transport in Radiative Nanofluids by Considering the Influence of Convective Heat Condition. *J Nanomater* (2022) 2022:1–11. doi:10.1155/2022/1854381
26. Adnan Ashraf W, Khan I, Anduaem M. Thermal Transport Investigation and Shear Drag at Solid-Liquid Interface of Modified Permeable Radiative-SRID Subject to Darcy-Forchheimer Fluid Flow Composed by  $\gamma$ -nanomaterial. *Sci Rep* (2022) 12. doi:10.1038/s41598-022-07045-2
27. Adnan Khan I, Shemseldin MA, Mousa AAA. Numerical Energy Storage Efficiency of MWCNTs-Propylene Glycol by Inducing Thermal Radiations and Combined Convection Effects in the Constitutive Model. *Front Chem* (2022) 10. doi:10.3389/fchem.2022.879276
28. Animasaun IL, Sandeep N. Buoyancy Induced Model for the Flow of 36 Nm Alumina-Water Nanofluid along Upper Horizontal Surface of a Paraboloid of Revolution with Variable thermal Conductivity and Viscosity. *Powder Tech* (2016) 301:858–67. doi:10.1016/j.powtec.2016.07.023
29. Ahmed N, Adnan Khan U, Khan I, Nisar KS. Heat and Mass Transfer in Magneto-Newtonian Fluid Past a Paraboloid of Revolution with Internal Heat Source. *Jmag* (2020) 25(2):254–61. doi:10.4283/jmag.2020.25.2.254

**Conflict of Interest:** The authors declare that the research was conducted in the absence of any commercial or financial relationships that could be construed as a potential conflict of interest.

**Publisher's Note:** All claims expressed in this article are solely those of the authors and do not necessarily represent those of their affiliated organizations, or those of the publisher, the editors, and the reviewers. Any product that may be evaluated in this article, or claim that may be made by its manufacturer, is not guaranteed or endorsed by the publisher.

Copyright © 2022 M. Alharbi, Adnan, Tag-Eldin, F. Yassen, Ahmed and Khan. This is an open-access article distributed under the terms of the Creative Commons Attribution License (CC BY). The use, distribution or reproduction in other forums is permitted, provided the original author(s) and the copyright owner(s) are credited and that the original publication in this journal is cited, in accordance with accepted academic practice. No use, distribution or reproduction is permitted which does not comply with these terms.